doi:10.14311/ppt.2025.2.123
*Plasma Physics and Technology* **12**(2):123–129, 2025


# PERFORMANCE EVALUATION OF MODIFIED TURBULENT MODELS IN SIMULATING ARC QUENCHING PROCESS IN CIRCUIT BREAKERS

Yujiao Qiao, Shanika Matharage, Zhongdong Wang*

*Department of Electrical and Electronic Engineering, The University of Manchester, Manchester, M13 9PL*

* Zhongdong.wang@manchester.ac.uk

**Abstract.** Gas circuit breakers rely on rapid gas expansion and turbulent mixing within a converging–diverging nozzle to effectively cool and extinguish arcs during current interruption. The transient arc interruption process involves coupled physical phenomena, including turbulent flow, electric current, convection and radiation. Selection of a suitable flow model is vital in obtaining simulation results matching the experimental data. In this study, the transient behaviour of the $SF_6$ flow during the current ramp-down phase is investigated. Performance of the standard k-$\epsilon$ turbulence model is compared with modified k-$\epsilon$ models, in which the turbulence dissipation constant $C_{1\epsilon}$ is systematically varied to identify the effect on the cooling process. Simulation results demonstrate that the adjustment of $C_{1\epsilon}$ can improve the arc cooling process by enhancing turbulent kinetic energy, resulting in maximum rate-of-rise of recovery voltage (RRRV) estimation values similar to the experimental conditions.

**Keywords:** Turbulent model, rate of rise of recovery voltage, gas circuit breaker.

## 1. Introduction

Gas circuit breakers are widely utilised in high-voltage power transmission due to their excellent arc-quenching capabilities and dielectric strength. During operation, an electric arc forms as the electrodes separate, heating the gas into a plasma. Gas flow is forced through a converging–diverging nozzle, undergoing rapid expansion and turbulent mixing, which cools and extinguishes the arc [1]. Arc quenching performance of a circuit breaker can be evaluated through simulating the transient behaviour and cooling effectiveness during the current ramp-down phase [2]. Computational fluid dynamics (CFD) simulations, employing either laminar or turbulence models, are used to investigate complex flow phenomena [3]. In simpler flow regimes or preliminary design stages, laminar flow models can provide insight into baseline pressure and temperature fields [4]. The turbulence models, such as the standard k-$\epsilon$ turbulence model, are applied to capture shear-driven mixing and eddy formation [5]. However, its performance significantly deteriorates in flows exhibiting strong compressibility, rapid strain, and pronounced adverse pressure gradients [6].

To enhance predictive accuracy under these challenging flow conditions, modified versions of the k-$\epsilon$ turbulence model, such as the Chen-Kim and RNG models, have been developed. The Chen-Kim model introduces an additional production-scale term into the $\epsilon$-equation to better capture non-equilibrium turbulent phenomena, especially flows with high strain and separation [7]. The RNG k-$\epsilon$ model provides improved predictions in rapidly strained and compressible flows by using modified transport equations and empirically adjusted constants [6]. Besides, modifications to the standard k-$\epsilon$ model have been explored by adjusting its empirical turbulence constants [8], which govern the production rate of turbulence dissipation. Decreasing these constants typically enhances turbulence dissipation, influencing turbulent mixing rates and cooling performance [9, 10]. In [11], an arc plasma model using finite volume method (FVM) was built to simulate 550 kV 80 kA circuit breaker. Evaluating different values of $C_{1\epsilon}$ it suggested that $C_{1\epsilon} = 1.44$ is suitable as it resulted in a distinct and smooth arc profile with a relatively stable arc temperature and moderate central arc pressure compared to the other two values. However, the optimal adjustment of this constant often depends on software specifics, nozzle geometry, and flow conditions [7, 12]. FVM integrates governing equations over control volumes, ensuring exact conservation of mass, momentum, and energy across cell boundaries. FEM focuses on accuracy through variational formulations but does not inherently guarantee strict local conservation without special modifications. Over the years, FEM has developed to solve fluid dynamics through advanced stabilization techniques such as Streamline Upwind/Petrov–Galerkin (SUPG) and specialized methods like the Discontinuous Galerkin Finite Element Method (DG-FEM) [13]. FVM is widely used for fluid dynamics, when considering coupling physics, the finite element method (FEM) has good performance.

This study use FEM to simulate arc, which this method is suited to handle the tightly coupled multiphysics interactions of electromagnetic forces, gas dynamics, and thermal expansion. This paper presents a numerical investigation on the application of turbulence models to study the arc quenching process in an $SF_6$ gas circuit breaker nozzle through FEM, using high Mach number module in COMSOL Multiphysics software. This study compares the performance of standard and modified k-$\epsilon$ models in estimating the

maximum rate of rise of recovery voltage.

## 2. Methodology of arc model

### 2.1. Governing equations

The time-averaged mass conservation:

$$\frac{\partial \rho}{\partial t} + \nabla\cdot(\rho\,\vec{V}) = 0 \tag{1}$$

where $t$ is time, $\rho$ is density, $\vec{V}$ is velocity.

Time-averaged momentum conservation equation:

$$\rho\,\frac{\partial \vec{V}}{\partial t} + \rho\,(\vec{V}\cdot\nabla)\,\vec{V} = -\nabla\cdot(p\,I) + \nabla\cdot\bar{\tau} + \vec{F} \tag{2}$$

$$\bar{\tau} = \mu\Big[(\nabla\vec{V} + (\nabla\vec{V})^T) - \tfrac{2}{3}\,(\nabla\cdot\vec{V})\,I\Big] - \tfrac{2}{3}\,\rho\,k\,I \tag{3}$$

$$\mu = \mu_t + \mu_\ell \tag{4}$$

where $p$ is pressure, $\tau$ is viscous stress tensor, $\vec{F}$ is additional force per unit volume, $\mu$ is dynamic viscosity, $\mu_l$ is dynamic molecular viscosity, $\mu_t$ is dynamic turbulent viscosity, $I$ is identity tensor.

Time-averaged energy conservation equation:

$$\rho\,C_p\Big(\frac{\partial T}{\partial t} + (\vec{V}\cdot\nabla)T\Big) = -\nabla\cdot q_k + Q_{vd} - Q_p + Q \tag{5}$$

where $C_p$ is specific heat capacity, $T$ is absolute temperature, $q_k$ is heat flux, $Q_{vd}$ is viscous heating, $Q_p$ is pressure work, and additional term $Q$ is heat source combining ohmic heating and radiation. Calculation of $q_k$, $Q_{vd}$, $Q_p$ and $Q$ are shown as follows:

$$q_k = k_q\,\nabla T \tag{6}$$

$$Q_{vd} = \sum_{i,j}\tau_{ij}\,\frac{1}{2}\Big(\frac{\partial V_i}{\partial x_j} + \frac{\partial V_j}{\partial x_i}\Big) \tag{7}$$

$$Q_p = -\frac{1}{\rho}\,\frac{\partial \rho}{\partial T}\bigg|_p\,T\,\Big(\frac{\partial p}{\partial t} + \vec{V}\cdot\nabla p\Big) \tag{8}$$

$$Q = \sigma\,E^2 - q_{\mathrm{nec}} \tag{9}$$

where $k_q$ is thermal conductivity, $E$ is electric field, $\sigma$ is electrical conductivity and $q_{nec}$ is radiated energy per unit volume.

The above equations are supplemented by the equation of state, which is usually expressed as

$$\rho = f(p, T) \tag{10}$$

where $\rho$ is density, $p$ is pressure, $T$ is temperature. The transport properties, dynamic viscosity $\mu$, thermal conductivity $k_q$, and electrical conductivity $\sigma$, are functions of temperature and pressure [14].

### 2.2. Turbulence model

Turbulence plays a major role in arc cooling within gas blast interruption theories [15]. Turbulence is created by the shear layer between the fast-flowing hot plasma in the arc core and the much slower and cooler gas outside that region. Introducing turbulence into the flow field improves arc interruption behaviour [16]. The standard k-$\epsilon$ model is the most widely used turbulence model for engineering applications. It gives a general description of the conversion of the energy from the mean flow to chaotic turbulence for the maintenance of turbulent flow and the dissipation of turbulence energy extracted from the mean flow [17]. The standard k-$\epsilon$ model has two transport equations, one of which describes the conservation of turbulent kinetic energy ($k$) per unit mass, which represents the energy contained in turbulence. The other describes the turbulence dissipation rate ($\epsilon$), which describes the rate at which turbulence energy is converted into thermal energy [18]. Besides, the model relies on five key empirical parameters, $C_{1\epsilon}$ (1.44), $C_{1\epsilon}$ (1.92), $C_\mu$ (0.09), $\sigma_k$ (1.0), and $\sigma_e$ (1.3) which have been derived from experimental observations.

$$\frac{\partial(\rho\,k)}{\partial t} + \nabla\cdot(\rho\,k\,\bar{\vec{V}}) = \nabla\cdot\Big(\big(\mu_l + \tfrac{\mu_t}{\sigma_k}\big)\,\nabla k\Big) + G_k - \rho\,\varepsilon \tag{11}$$

$$\frac{\partial(\rho\,\varepsilon)}{\partial t} + \nabla\cdot(\rho\,\varepsilon\,\bar{\vec{V}}) = \nabla\cdot\Big(\big(\mu_l + \tfrac{\mu_t}{\sigma_\varepsilon}\big)\,\nabla\varepsilon\Big) + C_{1\varepsilon}\,\frac{\varepsilon}{k}\,G_k + C_{2\varepsilon}\,\rho\,\frac{\varepsilon^2}{k} \tag{12}$$

where $\rho$ is gas density, $k$ is turbulent kinetic energy, $\bar{\vec{V}}$ is mean velocity, $\mu_l$ is dynamic (molecular) viscosity, $\mu_t$ is dynamic (turbulent) viscosity, $G_k$ is production of turbulent kinetic energy, $\varepsilon$ is turbulence dissipation rate, $C_{1\varepsilon}$ controls turbulence production in the dissipation-rate equation, $C_{2\varepsilon}$ governs turbulence dissipation, $\sigma_k$ is turbulent Prandtl number for $k$ (regulating its diffusion), and $\sigma_\varepsilon$ is turbulent Prandtl number for $\varepsilon$.

Dynamic turbulent viscosity is calculated by

$$\mu_t = \rho\,C_\mu\,\frac{k^2}{\varepsilon} \tag{13}$$

where $C_\mu$ is a coefficient used to compute the eddy viscosity.

The generation of the turbulent kinetic energy $G_k$ is related to the rate of strain in an axisymmetric arc:

$$G_k = \mu_t\Big[2\Big(\frac{\partial w}{\partial z}\Big)^2 + 2\Big(\frac{\partial v}{\partial r}\Big)^2 + 2\Big(\frac{v}{r}\Big)^2 + \Big(\frac{\partial w}{\partial r} + \frac{\partial v}{\partial z}\Big)^2\Big] \tag{14}$$

where $\mu_t$ is dynamic turbulent viscosity, $w$ is velocity component of the $z$ direction, and $v$ is velocity component of the $r$ direction.

In addition to the standard k-$\epsilon$ model, two modified k-$\epsilon$ models were studied by varying the $C_{1\varepsilon}$ term, which has been utilised to optimise simulation results in other literature [10, 12]. In general, $C_{1\epsilon}$ in (12) is

proportional to the turbulence dissipation rate. Therefore, decreasing it would result in an increase in the turbulence kinetic energy, which in turn enhances the turbulent exchange. Hence, the effect of the turbulence dissipation constant $C_{1\epsilon}$ was studied by varying ±15% range around the standard k-$\epsilon$ model 1.44, which is consistent with other modified k-$\epsilon$ variants (the RNG model uses 1.42, and Chen–Kim employs 1.15). Results from the model with modified parameters 1.24 and 1.64 are compared with the results from standard k-$\epsilon$ model. This limited sweep ensures the modified model stays within a plausible range. The transient behaviour of the $SF_6$ switching arc during the current ramp-down is evaluated by examining Mach number, temperature, turbulent kinetic energy, and arc radius profiles.

Besides, the radiation is calculated based on the NEC model, which was introduced by Liebermann and Lowke [19]. It is a commonly used model to quantify the radiative energy losses during arc quenching [20]. The model incorporates two distinct regions. The arc core region, which emits radiation and the surrounding reabsorption region in which some of the emitted radiation is reabsorbed by the arc column [19].

## 2.3. Modelling of supersonic flowl

COMSOL Multiphysics discretises PDEs by applying FEM. FEM converts each equation into a weak form through test functions, integrates over mesh elements, and approximates the solution with nodal values and polynomial shape functions to form a global sparse system [13]. Accuracy is tuned through mesh refinement or higher-order elements, and after setting boundary conditions, COMSOL uses direct or iterative solvers with adaptive meshing and error estimators to ensure convergence [21]. CFD package in COMSOL is capable of simulating compressible flow.

### 2.3.1. Nozzle geometry

The geometry was extracted based on the Laval nozzle used for experiments conducted in [22]. The model dimensions were extracted from the drawing provided in [22] and was implemented as 2D axis symmetry model in the Finite Element Method (FEM) software. Figure 1 shows the nozzle structure with upstream and downstream electrodes. The contact material was set as copper-tungsten (Cu-W). The upstream has an electrode with a rounded tip, while the downstream has a hollow electrode.

### 2.3.2. Boundary conditions

The boundary conditions are specified at the nozzle inlet, nozzle outlet, nozzle wall, and upstream electrode.

1. Pressure is set at the inlet and outlet boundary, which were derived from experiments in [22].

2. A non-slip boundary condition for velocity is applied to the wall surface, and the surface is set to be adiabatic [23].

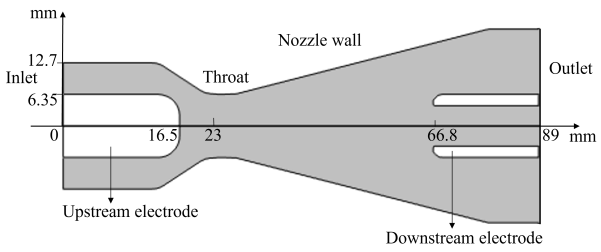


*Figure 1. Laval nozzle geometry.*

| Boundary condition | Values |
|---|---|
| Inlet pressure | 13.6 atm |
| Outlet pressure | 3.4 atm |
| DC | 1000 A |
| Current ramp down | From 1000 A with rate 13 A/$\mu$s |

*Table 1. Boundary conditions and values in simulation.*

3. The current density [7] and current ramp-down rate are applied to the surface of the upstream electrode.

4. The thermal conduction in the solid is considered in electrodes.

5. At the arc symmetry, there is no normal or shear flow and no mass, heat, or turbulence transport across the boundary, and both the electric potential and current density exhibit no variation normal to the symmetry boundary.

The simulation condition is a current ramp down from 1000 A to 0 A with a rate of 13 A/µs. The boundary conditions in the simulation are shown in Table 1. The effect of contact erosion and nozzle ablation was not considered in the simulation.

### 2.3.3. Simulation procedure

For each flow model, the simulation was started with cold flow condition in which the flow was established without an arc. The steady-state cold flow results were then used as the initial condition to incorporate the arc into the switching arc simulation, which is the DC arc stage. The DC arc stage presents the fully developed arc under continuous current. Following the transient study of the current ramp-down simulation is initiated with a stable DC arc. During the simulation, the current ramped down from a stable DC arc to 0 A with a fixed rate. The last stage is the transient recovery voltage stage, the rate of rise of recovery voltage (RRRV) is applied between the two electrodes to test arc clearance or reignition by evaluating the change in arc resistance with time, as proposed in [5]. When the arc resistance increases with time to an infinite value, the arc is distinguished. In contrast, the resistance first slightly increases with time, then decreases to almost zero, which means the arc is reignited between the electrodes.

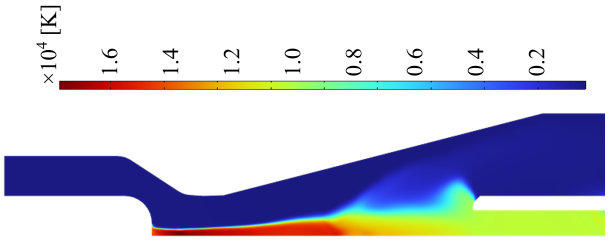


*Figure 2. Temperature distribution at 1000 A DC, standard k-ϵ model.*

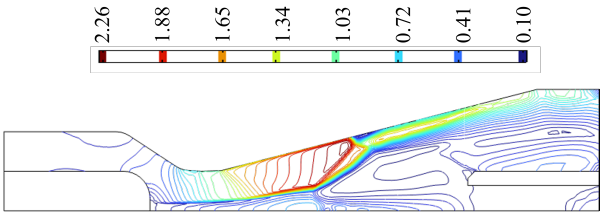


*Figure 3. Mach number contour at 1000 A DC, standard k-ϵ model.*

## 3. Results and discussion of arc simulation

### 3.1. Effect of $C_{1\epsilon}$ parameter on the DC arc simulation

The temperature distribution of the arc at 1000 A obtained for the standard k-ϵ model is shown in Figure 2. The energy in the arc model includes the energy input through Ohmic heating and the energy dissipation, which occurs through convection, thermal conduction, radiation, pressure work and viscous work. The arc exhibits a wider radius (distance from symmetry axis to 4000 K) near the upstream electrode, and then the arc shrinks at the throat area. As the arc progresses downstream, the radius gradually increases due to the influence of the radial convection within the nozzle. The temperature profile reveals that the highest temperatures are concentrated along the axial symmetry axis, where Ohmic heating is most intense. In the arc core region, the temperature distribution remains relatively uniform along the radial direction. The arc boundary is defined in the NEC model by electrical boundary ($R_2$), the location at which the electric conductivity equals one, which is usually considered to be at 4000 K.

Figure 3 shows the Mach number distribution in the nozzle. The flow in the Laval nozzle is supersonic, and a shock appears in the downstream area. The Mach number increases from the inlet through the throat to the downstream area and reaches a maximum Mach number of 2.26 before the shock. In the arc area, due to the high temperature and high speed of sound, the Mach number is lower than in the surrounding cooler area.

Figure 4 shows the temperature distribution along the z-axis of symmetry boundary for the standard

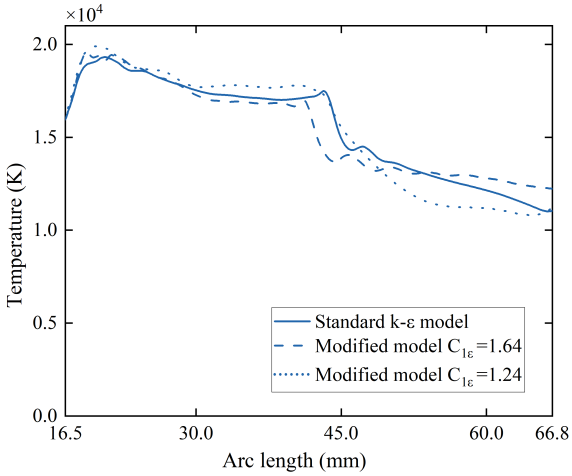


*Figure 4. Comparison of temperature at symmetry along the z-axis of the standard k-ϵ model, modified $C_{1\epsilon}$=1.24 and modified $C_{1\epsilon}$=1.64 at 1000 A DC.*

k-ϵ model, modified $C_{1\epsilon}$=1.24 and modified $C_{1\epsilon}$=1.64. Prior to the shock, the temperature distribution is similar for all three models. The temperature of all three models drops sharply after the shock due to the lower velocity and smaller heat dissipation through convection. The model with $C_{1\epsilon}$=1.24 has a slightly larger drop in temperature along the z-axis, which could be due to this region being more influenced by turbulent kinetic energy.

### 3.2. Effect of $C_{1\epsilon}$ parameter on current ramp down and RRRV of arc simulation

Figure 5 illustrates the radial temperature distribution at a point (23 mm) selected in the nozzle throat region at three distinct instants current (50 A, 10 A, and 0 A) during the current ramp-down process from 1000 A to 0 A at a rate of 13 A/µs. At the current condition 0 A, the lower value $C_{1\epsilon}$=1.24 exhibited notably reduced temperatures in the arc core region (close to the symmetry boundary). However, at higher current (50 A), this same setting did not yield improved cooling relative to the standard model. This behaviour can be attributed to the distinct physical mechanisms governing energy transfer at different current magnitudes. At high current and elevated arc core temperature, radiative energy transfer dominates heat dissipation. Conversely, as the arc temperature drops to below approximately $1\times10^4$ K, heat transfer through convection increases [5]. Therefore at lower current values (10 A and 0 A), the enhanced turbulent mixing associated with a lower $C_{1\epsilon}$ value causes a rapid reduction in the temperature at the arc core. At 0 A, the maximum temperature of the modified $C_{1\epsilon}$=1.24 model is 8% lower than the standard k-ϵ model whereas for the model with $C_{1\epsilon}$=1.64 was 3% higher than the standard k-ϵ model.

Figure 6 shows the temperature distribution along the z-axis during current ramp down at instances

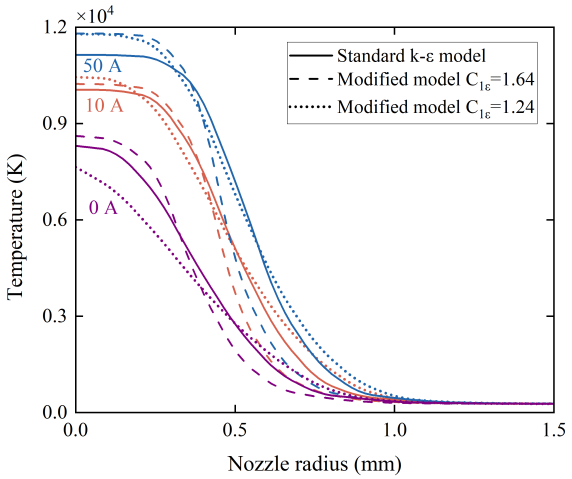


*Figure 5. Comparison of temperature distribution at a throat location (23 mm from inlet) along the radial direction of the standard k-ϵ model, modified $C_{1\epsilon}$=1.24 and modified $C_{1\epsilon}$=1.64 at instant current 50 A, 10 A and 0 A during current ramp down.*

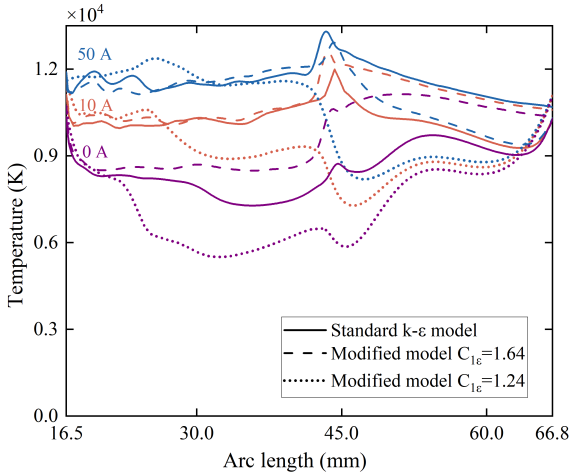


*Figure 6. Comparison of temperature at symmetry along the z-axis of the standard k-ϵ model, modified $C_{1\epsilon}$=1.24 and modified $C_{1\epsilon}$=1.64 at instant current 50 A, 10 A and 0 A during current ramp down.*

of 50 A, 10 A and 0 A obtained for all three models. While under steady-state (DC arc) conditions, all three models showed similar axial temperature in the region before the shock (Figure 4 ), differences emerge as the current is ramped down, close to current zero.

At 50 A current all three models exhibited similar temperature profiles in the region before the shock, with the model with modified $C_{1\epsilon}$=1.24 exhibiting a maximum of 8.7% deviation compared to the standard k-ϵ model. In contrast, in the region after the shock, the temperature obtained from the model with modified $C_{1\epsilon}$ is considerably lower (up to 27.9%) compared to standard k-ϵ model.

At 0 A, a clear deviation can be observed among all three models with the modified $C_{1\epsilon}$=1.24, having a lower temperature profile compared to the standard k-ϵ model and the model with modified $C_{1\epsilon}$=1.64, having a higher temperature profile. Considering the whole axial length, the model with a modified $C_{1\epsilon}$=1.24 has up to 25.3% lower temperature compared to the standard k-ϵ model. On the other hand, the model with a modified $C_{1\epsilon}$=1.64 has up to 27% higher temperature compared to the standard k-ϵ model. Results indicate that the model with a modified $C_{1\epsilon}$=1.24 promotes greater convective heat transfer in the throat area and downstream area compared to the other two models.

Figure 7 illustrates the turbulence kinetic energy (calculated from (12)) at the throat along the radial direction of the three models at the current zero condition. The decrease of $C_{1\epsilon}$, results in an increase in turbulence kinetic energy largely. The highest value of turbulence kinetic energy of the modified $C_{1\epsilon}$=1.24 is almost twice the standard k-ϵ model and five times higher than the modified $C_{1\epsilon}$=1.64.

Figure 8 illustrates the dynamic viscosity (calculated from (13))at the throat along the radial direction

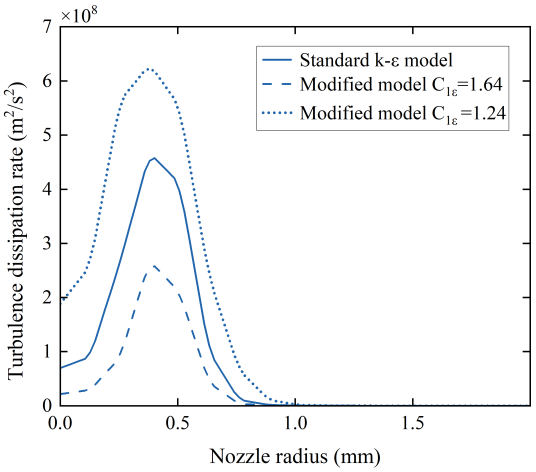


*Figure 7. Comparison of turbulence kinetic energy at the throat along the radial direction of the standard k-ϵ model, modified $C_{1\epsilon}$=1.24 and modified $C_{1\epsilon}$=1.64 at instant current 0 A during current ramp down.*

of the three models. Decreasing $C_{1\epsilon}$ causes the increase in the turbulence dynamic viscosity ($\mu_t$). Modified $C_{1\epsilon}$=1.24 is three times higher than the standard k-ϵ model. Increase in dynamic viscosity ($\mu_t$) indicates increase in the mixing of gas flow into the arc core, resulting in a more strongly accelerated supersonic flow.

Figure 9 shows turbulence kinetic energy profiles at the symmetry boundary along the z-axis direction obtained for 0 A. The model with modified $C_{1\epsilon}$=1.24 shows higher amplitude across the nozzle, indicating that the peak of turbulence kinetic energy appears earlier than the other two models, which indicates the turbulence is dissipating energy more rapidly compared to the other models.

Figure 10 shows the comparison of the maximum

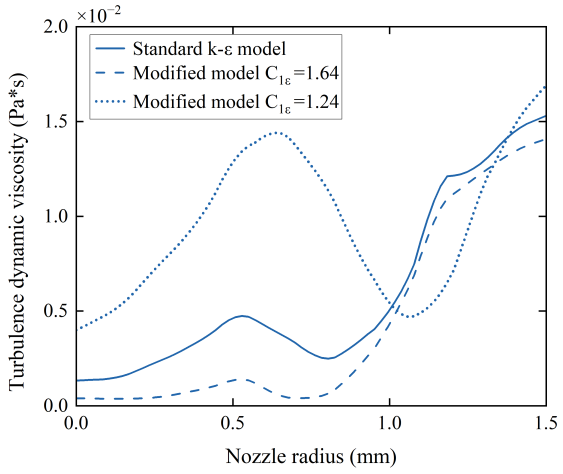


*Figure 8. Comparison of turbulence dynamic viscosity at the throat along the radial direction of the standard k-ϵ model, modified $C_{1\epsilon}$=1.24 and modified $C_{1\epsilon}$=1.64 at instant current 0 A during current ramp down.*

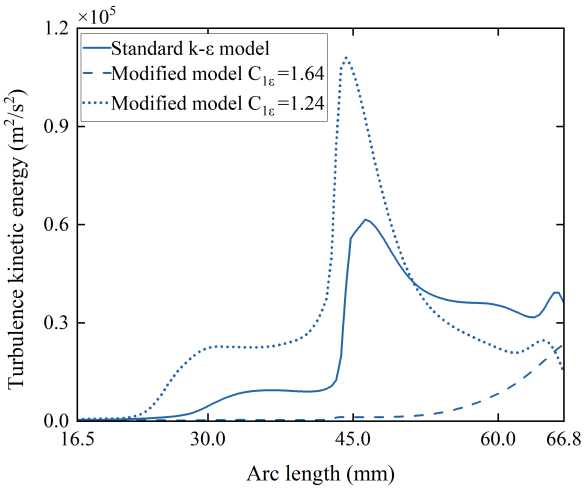


*Figure 9. Comparison of turbulence kinetic energy at symmetry along the z-axis of the standard k-ϵ model, modified $C_{1\epsilon}$=1.24 and modified $C_{1\epsilon}$=1.64 at instant current 0 A during current ramp down.*

rate of rise of recovery voltage (RRRV) before breakdown obtained from experimental data and simulation models. The standard k-ϵ model indicates 25% lower RRRV compared to experimental data. The turbulence model with modified $C_{1\epsilon}$=1.24 showed best performance in estimating RRRV with only a 2.5% difference against the measured value. With increasing $C_{1\epsilon}$, RRRV decreases because of higher temperature at 0 A and lower turbulence exchange ability.

## 4. Conclusions

Through FEM method, the paper studied the potential of modifying turbulent parameter ($C_{1\epsilon}$) in the standard k-ϵ turbulence model to improve the accuracy of estimating the maximum RRRV in a circuit breaker that consists of converging-diverging Laval-

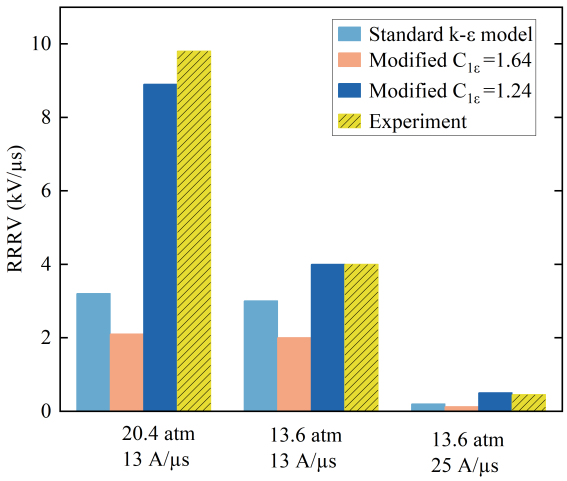


*Figure 10. Comparison of the rate of rise of recovery voltage of the standard k-ϵ model, modified $C_{1\epsilon}$=1.24 and modified $C_{1\epsilon}$=1.64 with experimental data under three conditions.*

type nozzle. Results from standard k-ϵ model against two modified variants, $C_{1\epsilon}$ set to 1.24 and 1.64. Compared to standard k-ϵ model, the modified model with $C_{1\epsilon}$=1.24 showed an improvement in estimating the maximum RRRV through the increase in dynamic viscosity and turbulent kinetic energy. The increase in dynamic viscosity allows increase in the mixing of gas flow into the arc core, resulting in a more strongly accelerated supersonic flow supporting the cooling process. Also the stronger production of turbulence kinetic energy along both axial and radial directions promotes rapid dissipation of energy through turbulence. As a result, core temperatures fall rapidly at low current near 0 A, resulting in an improved RRRV. This indicates that single-parameter modification to the k-ϵ model can improve the predictive accuracy of CFD simulations for the Laval nozzle of the $SF_6$ circuit breaker. Future work will explore the approach across a wider range of operating conditions.

## References

[1] H. Ito. *Switching Equipment.* CIGRE, Paris, France, 2019.

[2] M. L. Wu, F. Yang, and M. Z. Rong. Numerical study of turbulence-influence mechanism on arc characteristics in an air direct current circuit breaker. *Physics of Plasmas*, 23(4):042306, 2016. doi:10.1063/1.4943285.

[3] X. Ye, M. T. Dhotre, J. D. Mantilla, and S. Kotilainen. Cfd analysis of the thermal interruption process of gases with low environmental impact in high voltage circuit breakers. In *2015 IEEE Electrical Insulation Conference (EIC)*, pages 375–378, 2015.

[4] B. Lu, L. Xu, and X. Zhang. Three-dimensional mhd simulations of the electromagnetic flowmeter for laminar and turbulent flows. *Flow Measurement and Instrumentation*, 33:239–243, 2013. doi:J.FLOWMEASINST.2013.07.015.

[5] K. Zhang, S. Yao, Y. Wu, and J. D. Yan. A method for analysing and characterizing the arc cooling effect of different gases in strong axial flow with $sf_6$ and air as examples. *IEEE Transactions on Power Delivery*, pages 1–11, 2023.

[6] V. Yakhot and S. A. Orszag. Renormalization group analysis of turbulence. i. basic theory. *Journal of Scientific Computing*, 1(1):3–51, 1986. doi:10.1007/BF01061452.

[7] J. Liu. *Modelling and simulation of air and $SF_6$ switching arcs in high voltage circuit breakers*. Ph.d. thesis, Department of Electrical Engineering and Electronics, University of Liverpool, Liverpool, United Kingdom, 2016.

[8] Y. J. Kim and J. C. Lee. Comparison of turbulence models for a free-burning high-intensity argon arc. *Journal of the Korean Physical Society*, 62(9):1252–1257, 2013. doi:10.3938/jkps.62.1252.

[9] Y. S. Chen and S. W. Kim. Computation of turbulent flow using an extended turbulence closure model. Technical Report 88, NASA STI/Recon Technical Report N, November 1987.

[10] P. A. Davidson. *Turbulence: An Introduction for Scientists and Engineers*. Oxford University Press, Oxford, United Kingdom, 2004. ISBN 978–0–19–872258–8.

[11] Y. Zheng, F. Zhou, C. Gao, et al. Optimization of c1 parameter in arc plasma turbulence simulation: Based on energy balance and turbulence characteristics. In *2024 7th International Conference on Electric Power Equipment - Switching Technology (ICEPE-ST)*, pages 774–779, 2024.

[12] J. D. Yan, K. I. Nuttall, and M. T. C. Fang. A comparative study of turbulence models for $SF_6$ arcs in a supersonic nozzle. *Journal of Physics D: Applied Physics*, 32(12):1401–1406, 1999. doi:10.1088/0022-3727/32/12/317.

[13] COMSOL. *CFD Module User's Guide*. COMSOL, 2017. User's Guide.

[14] L. Frost and R. Liebermann. Composition and transport properties of $SF_6$ and their use in a simplified enthalpy flow arc model. *Proceedings of the IEEE*, 59(4):474–485, 1971. doi:10.1109/PROC.1971.8206.

[15] W. Hermann. Experimental and theoretical study of a stationary high-current arc in a supersonic nozzle flow. *Journal of Physics D: Applied Physics*, 7(12):1703, 1974. doi:10.1088/0022-3727/7/12/317.

[16] W. Hermann, U. Kogelschatz, K. Ragaller, and E. Schade. Investigation of a cylindrical, axially blown, high pressure arc. *Journal of Physics D: Applied Physics*, 7(4):607, 1974. doi:10.1088/0022-3727/7/4/315.

[17] W. Hermann, U. Kogelschatz, L. Dr Niemeyer, et al. Investigation on the physical phenomena around current zero in HV gas blast breakers. *IEEE Transactions on Power Apparatus and Systems*, 95(4):1165–1176, 1976. doi:10.1109/T-PAS.1976.32210.

[18] Y. A. Çengel and J. M. Cimbala. *Fluid Mechanics Fundamentals and Applications*. McGraw-Hill Education, New York, USA, 4 edition, 2017. ISBN 9780073044651.

[19] R. W. Liebermann and J. J. Lowke. Radiation emission coefficients for sulfur hexafluoride arc plasmas. *International Journal of Quantitative Spectroscopy and Radiative Transfer*, 16(3):253–264, 1976. doi:10.1016/0022-4073(76)90067-4.

[20] V. Aubrecht and M. Bartlova. Net emission coefficients of radiation in air and $SF_6$ thermal plasmas. *Plasma Chemistry and Plasma Processing*, 29(2):131–147, 2009. doi:10.1007/s11090-008-9163-x.

[21] COMSOL. *COMSOL Reference Manual*. COMSOL, 2019. Reference Manual.

[22] G. Frind, J. A. Rich, R. E. Kinsinger, et al. Fundamental investigation of arc interruption in gas flows. Technical report, New York, 1977.

[23] S. K. Park, K. Y. Park, and H. J. Choe. Flow field computation for the high voltage gas blast circuit breaker with the moving boundary. *Computer Physics Communications*, 177(9):729–737, 2007. doi:10.1016/j.cpc.2007.07.004.